communications medicine

A Nature Portfolio journal

Article

https://doi.org/10.1038/s43856-025-01238-2

Patient-specific musculoskeletal modeling to enhance preoperative planning for pelvic fracture reduction

Jixuan Liu[1], Yufeng Ge[2], Sutuke Yibulayimu[3], Yanzhen Liu[3], Xinbao Wu[2] ✉, Yu Wang[3] ✉ & Yuanwei Zheng[4]

Abstract

Background Pelvic fracture surgery is a highly complex and skill-dependent procedure due to adjacent neurovascular structures. These challenges often result in prolonged operative time, elevated complication rates, and repeated reduction attempts. To support surgeons in overcoming these difficulties, our study introduces a rapid modeling approach that enables precise preoperative planning and quantitative evaluation of reduction strategies.

Methods We developed an automated patient-specific modeling method that integrates Statistical Shape Models with the personalized modeling modules of the OpenSim software's Application Programming Interface for generating personalized musculoskeletal models. Using this approach, we rapidly reconstructed reduction models for 10 patients (age range: 49-72) with pelvic fractures and validated the results against clinical reduction force data.

Results Here we show that the SMAG framework generates patient-specific models 78% faster than manual methods while reducing reconstruction errors to below 7.7%. Validation against clinical data demonstrates force prediction with an average error of 13.8%, within clinically acceptable limits (<10 N vs. typical 15–25 N traction force). Optimal reduction paths identified reduced peak forces from 555.4 N to 97.4 N.

Conclusions Our method transforms pelvic fracture management by translating surgical expertise into quantifiable, data-rich biomechanical parameters. This data-driven framework not only enables optimized surgical planning for both robotic and manual procedures but also provides a high-resolution quantitative basis for AI-enhanced decision support. By shifting the field from a subjective art to an objective science, our approach standardizes surgical outcomes and paves the way for intelligent systems that deliver more precise and higher-quality surgical planning.

Plain language summary

Surgery to repair a broken pelvis is very difficult and risky because the bones are near important nerves and blood vessels. To help surgeons plan these operations more safely, we created a computer tool that can quickly build a custom model of a patient's unique injury. Our tool uses software to analyze medical scans and create a digital map of the bones. We tested it on data from ten patients and found that it is much faster and more accurate than previous methods. Most importantly, it can simulate different ways to perform the surgery and show surgeons which method requires the least force, making the procedure much safer. This research is a step towards making complex surgery more predictable and less dependent on a surgeon's guesswork. In the future, such tools could help surgeons consistently choose the best plan for each patient, leading to better outcomes and faster recovery.

Fracture reduction is a critical procedure in orthopedic trauma surgery, requiring a delicate balance among bones, muscles, and soft tissues to achieve successful outcomes. Pelvic fractures, in particular, present formidable challenges due to the complex three-dimensional anatomy and intricate surrounding neurovascular structures[1–3]. These fractures are associated with sobering mortality (>13%) and morbidity (>60%) rates, reflecting their unique biomechanical complexity[4,5]. Unlike long bone fractures, managing pelvic injuries necessitates consideration of the irregular pelvic geometry and the multidirectional forces exerted by over 40 surrounding muscles[6]. Currently, orthopedic surgeons lack reliable intraoperative references for assessing reduction quality and mechanical performance, often leading to prolonged surgery times, multiple reduction attempts, and elevated reoperation rates. For instance, the average time for a pelvic reduction surgery in males can reach up to 260 min, resulting in

[1]Institue of Medical Equipment Science and Engineering (IMESE), Huazhong University of Science and Technology, Wuhan, China. [2]Department of Orthopedics and Traumatology, Beijing Jishuitan Hospital, Capital Medical University, Beijing, China. [3]School of Biological Science and Medical Engineering, Beihang University, Beijing, China. [4]School of Architecture and Urban Planning, Huazhong University of Science and Technology, Wuhan, China.
✉e-mail: wuxinbao_jst@126.com; wangyu@buaa.edu.cn

substantial physical strain on surgeons[7]. A one-year follow-up study of 194 patients reported that 48 patients (25%) required unplanned reoperations, with nerve injuries—frequently caused by excessive traction and manipulation during reduction—being the most common complication (34 cases, 18%)[8].

While advancements in artificial intelligence and robotic-assisted surgery have introduced new capabilities for pelvic fracture treatment, a significant gap persists in quantifying crucial mechanical parameters—such as reduction force and soft tissue impedance—during the procedure. The absence of real-time, patient-specific biomechanical feedback limits the full potential of these advanced technologies, affecting surgical fluency and safety. For instance, in robotic-assisted reduction, the inability to precisely anticipate tissue resistance hinders path optimization and compliance with safety force thresholds (the robotic arm's load usually below 160 N)[9,10].

Numerous articles have highlighted the importance of addressing mechanical issues during pelvic fracture reduction, whether in traditional or robotic surgery[8,11–13]. A major obstacle is the lack of rapid, precise, and clinically applicable mechanical evaluation methods[14]. Conventional solutions for mechanical evaluation, such as patient-specific musculoskeletal modeling[15–17], have been constrained by the labor-intensive and error-prone process[18] of manually annotating muscle attachment points. For example, a lower limb model incorporating the pelvis may involve up to 282 points[19]. These muscle attachment points, essential in muscle force-line models, delineate muscle pathways and characterize the direction of muscle force application. This modeling method excels in rigid body dynamics analysis and has been extensively validated for combining accuracy with efficiency[13,20,21]. Although medical imaging enables rapid skeletal reconstruction[22,23], generating accurate patient-specific muscle models remains a major bottleneck[24], preventing clinical adoption.

To address these challenges, we introduce the Statistical Musculoskeletal Automatic Generator (SMAG) framework—an innovative pipeline for end-to-end automation of patient-specific musculoskeletal modeling leveraging Statistical Shape Models (SSM). Unlike conventional scaling approaches, SMAG enables rapid, anatomically accurate reconstruction by automatically transferring pre-annotated muscle attachments from a baseline model to individual patient anatomy. Building on our team's extensive experience in robot-assisted pelvic fracture reduction—including system development[9,11] morphological analysis[25,26], and automatic planning[27]—this study integrates efficient patient-specific modeling with robotic-assisted surgery.

Here we show that the SMAG framework generates patient-specific models 78% faster than manual methods while reducing reconstruction errors to below 7.7%. Validation against clinical data demonstrates force prediction with an average error of 13.8%, while biomechanical analysis identifies reduction paths that lower peak resultant forces from over 550 N to below 100 N. These findings establish SMAG as an efficient and accurate solution for preoperative planning, enabling biomechanically-informed guidance that enhances the precision of robotic reduction, mitigates excessive resistance, and supports manual operations to improve clinical outcomes.

Methods

Overview of the SMAG Framework

The Statistical Musculoskeletal Automatic Generator (SMAG) framework was designed as an end-to-end automated pipeline for generating patient-specific musculoskeletal models of the pelvis and lower limbs. The overall workflow is illustrated in Fig. 1. Initially, a standard pelvic SSM was developed from 42 generic datasets, and attachment points for 23 sets of unilateral pelvic muscles were annotated. Subsequently, patient-specific musculoskeletal models were rapidly generated through adaptive matching technology applied to the SSM template. Then, Detailed mechanical analyses of the pelvic reduction process were performed using OpenSim software, encompassing the mechanical evaluation of various reduction strategies and the analysis of major muscle injuries.

Development of the Statistical Shape Model (SSM) and baseline musculoskeletal template

We leveraged ilium and sacrum data extracted from 40 open-source pelvic datasets to develop a statistical shape model[28,29]. The utilization of these de-identified images for secondary analysis was conducted under the ethical approval framework governing the original data source. Specifically, the datasets were obtained from The Cancer Imaging Archive (TCIA), whose establishment and distribution protocol was approved by the Washington University School of Medicine Institutional Review Board (IRB) under Protocol #201108194: "Image Archive Hosting". This approval encompassed the receipt and public sharing of de-identified data, with a waiver of the requirement for individual patient informed consent granted by the same IRB. The waiver was based on the minimal risk posed by the research, the impracticability of obtaining consent from subjects in a large-scale archive, and the implementation of robust, DICOM-standard-compliant de-identification processes that effectively protect patient privacy.

During the analysis of variations across these datasets, denoted as T(x), we distinguished between rigid and non-rigid differences. These were respectively quantified as $T_{global}(x)$ and $T_{local}(x)$, as delineated in Eq. 1. Rigid differences are primarily attributed to spatial positioning, rotation, and other non-morphological discrepancies within the data. In contrast, non-rigid differences relate to morphological variations, which are central to the statistical shape model. The initial step to develop a statistical shape model of the pelvis requires preprocessing of homologous datasets, which includes data cleansing, denoising, and sampling. These datasets are then normalized to create a training set designed to remove any variations in posture.(Fig. 2A)

$$\mathrm{T(x)} = \mathrm{T_{global}(x)} + \mathrm{T_{local}(x)} \tag{1}$$

In the STEP 2, the source point cloud undergoes rigid alignment with the target point cloud. Then, Gaussian radial basis functions combined with local elastic deformations are used for non-rigid registration. This process maps the template shape to other sample shapes, establishing point correspondences between the reference and sample point clouds[30]. Generalized Procrustes analysis (GPA) is utilized to neutralize the variances resulting from similarity transformations. The training dataset is denoted as $\mathrm{R} = \{\mathrm{R_i} | \ \mathrm{i} = 1, 2, \cdots, \mathrm{n}\}$, where 'n' represents the count of samples within the dataset. (Fig. 2B)

The STEP 3 builds upon the aligned shapes of the sample data, utilizing Gaussian Process Morphable Models (GPMM)[31]. A chosen skeletal shape serves as the reference Γ_R. Within this framework, we compute the mean function, $u_{SM}(x)$, and the covariance function, $k_{SM}(x, y)$, which characterize the Gaussian deformation processes involved. (Fig. 2C)

$$\mathbf{u_{SM}(x)} = \frac{\mathbf{1}}{\mathbf{n}}\sum_{\mathbf{i=1}}^{\mathbf{n}} \mathbf{u_i(x)} \tag{2}$$

$$\boldsymbol{k_{\mathrm{SM}}(x, y)} = \frac{\mathbf{1}}{\boldsymbol{n-1}}\sum_{i=1}^{n}\left(\boldsymbol{u_i(x)} - \boldsymbol{\mu_{\mathrm{SM}}(x)}\right)\left(\boldsymbol{u_i(y)} - \boldsymbol{\mu_{\mathrm{SM}}(y)}\right)^{T} \tag{3}$$

Herein, 'n' refers to the number of surface point clouds within the dataset. The term $u_i(x)$ describes the deformation at a point on the surface of the i_{th} sample. Following this, Principal Component Analysis (PCA)[32] is employed to perform dimensionality reduction on the covariance matrix. This process results in the parametric representation of the statistical shape model, denoted as $\boldsymbol{\Gamma_B}$:

$$\boldsymbol{\Gamma_B} = \{\mathbf{x} + \boldsymbol{\mu}(\mathbf{x}) + \mathbf{Pb_{ssm}} \mid \mathbf{x} \in \boldsymbol{\Gamma_R}\} \tag{4}$$

Herein, 'P' and 'b' correspond to the principal components and the weighting vector, respectively. The morphological parameters utilized in the skeletal model's Gaussian process deformation are captured by b_{ssm}. A

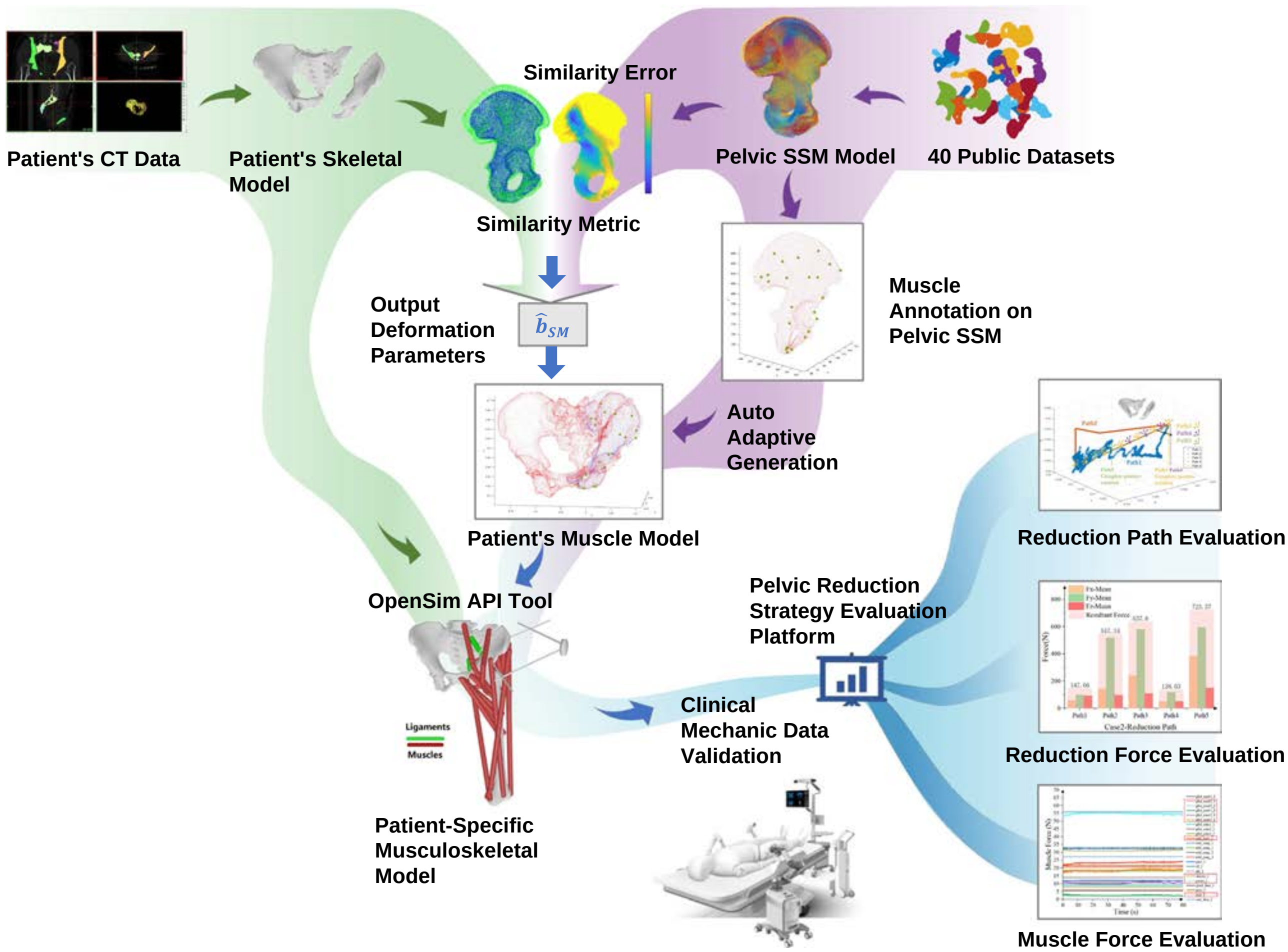

Fig. 1 | Framework for automated generation of patient-specific musculoskeletal models leveraging SMAG method and conducting mechanical evaluations of surgical strategies. Abbreviations: SSM Statistical Shape Model, SMAG Statistical Musculoskeletal Automatic Generator.

pivotal step in the personalized modeling process involves identifying a parameter set, b_{ssm}, that aligns with the patient's specific morphology.

Upon determining the optimal set of parameters, $\hat{b}_{ssm}$ the standard template, $\boldsymbol{\Gamma}_{\mathbf{B}}$, of the statistical shape model can be adapted into the patient's pelvic model, $\boldsymbol{\Gamma}_{\mathbf{R}}$, as delineated in Eq. (5).The iterative process initiates with the Iterative Closest Point (ICP) algorithm to make the template alignment. Subsequently, the point correspondences $\delta(x)$ between the $\boldsymbol{\Gamma}_{\mathbf{B}}$ and the patient's pelvis $\boldsymbol{\Gamma}_{\mathbf{R}}$ are established through the k-nearest neighbors' algorithm. Optimal match points are ascertained through bidirectional vertex correspondence. Ultimately, the parameters $\hat{b}_{ssm}$, which enable the adaptive deformation of the pelvic SSM to the patient's pelvic model, are determined. These parameters are confined within three standard deviations of the eigenvalue λ_i, as stipulated in parameter[33]. (Fig. 2C)

$$\hat{b}_{ssm} = \mathrm{argmin}\left(\delta(x) - \mu(x) - Pb_{SM}\right)\left|x \in \Gamma_R\right\}, \left|b_{ssm}\right| < \pm 3\sqrt{\lambda_i} \quad (5)$$

Figure 2C displays the clinical data from two patients included in this study, outlining the principal component analysis conducted to adaptively deform the standard sacrum and ilium SSM templates to the patient models. The bar chart enumerates the values of 39 principal component change parameters for each patient—blue bars represent Patient 1 and red bars represent Patient 2. It is evident that the parameters for adapting the standard iliac and sacral SSM templates to patient-specific skeletal changes exhibit significant differences, closely mirroring the individual skeletal transformations of each patient.

Patient-specific model generation via SSM matching

The reconstruction of patient-specific models requires clinical experts to annotate standard muscle and ligament attachment points on the canonical pelvic SSM (which has learned morphological variation characteristics from diverse healthy pelvises), serving as the baseline model for SSM transformation (gold standard). The annotation protocols followed Brand et al.'s clinical simplification framework[34]. Broad muscle groups, such as the gluteal complexes, were marked at functional centroids—a validated approach where deviations of ≤10 mm cause less than 10% moment arm errors. For tendon-constrained muscles, origins were mapped to osseous constraint sites like the lesser sciatic foramen, and insertions were mapped to functional zones such as the intertrochanteric crest. Furthermore, for hip-spanning muscles, only biomechanically essential attachment points were retained. The standard SSM pelvic model used in this study was constructed based on our previous work[25], which utilized the Open-Source Pelvis Atlas[29]—a repository of 40 pelvis CT segmentations and statistical shape models from I-STAR Lab, Johns Hopkins University.

The patient data used for pelvic fracture model reconstruction in this study were collected from Jishuitan Hospital in Beijing. The data collection was conducted under the clinical trial protocol titled "Evaluation of the effectiveness and safety of an orthopaedic surgical navigation system", which was approved by the Institutional Review Board of Jishuitan Hospital (Approval No.20210901). Written informed consent was obtained from all participating patients.

The first subject was a female in her early 50 s with a left sacroiliac joint dislocation, who underwent robot-assisted pelvic fracture reduction. The second subject was a female in her late 80 s with a left iliac wing

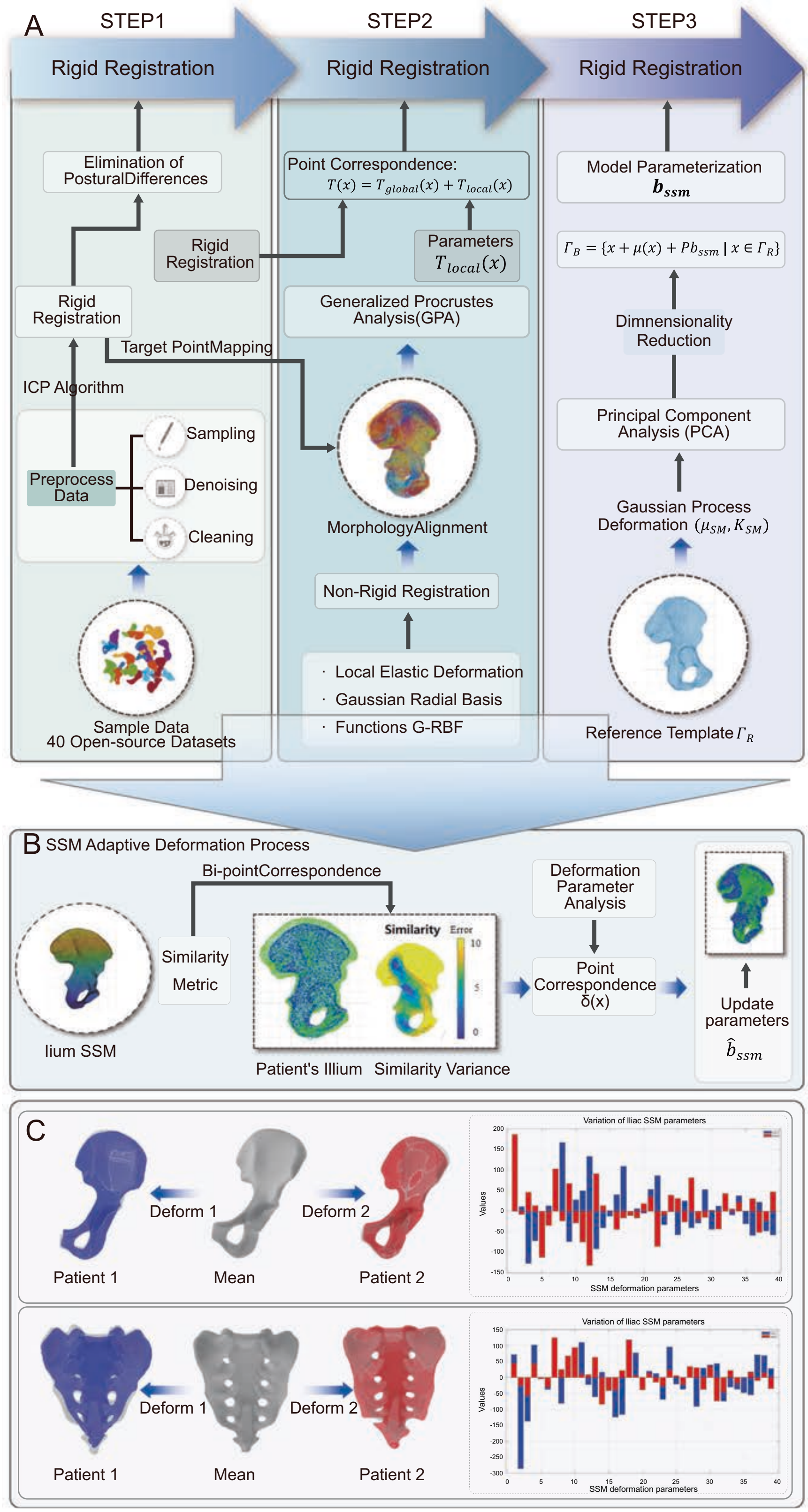

Fig. 2 | Construction and patient-specific adaptation of the statistical shape model (SSM). **A** Illustrative workflow of the ilium SSM construction process, detailing the steps to output the ilium SSM. **B** The adaptive deformation process utilizing the ilium SSM to conform to patient-specific iliac templates. **C** The principal component analysis of the deformation parameters $\hat{b}_{ssm}$, adapted to the patient-specific skeletal structure using SSM templates for two clinical cases. Blue bars indicate the deformation parameters for Patient 1, while red bars represent Patient 2, demonstrating significant variances in deformation parameters between the two patients. The SSM was built from a cohort of $N = 40$ subjects[28]. Abbreviations: ICP Iterative Closest Point, GPA Generalized Procrustes Analysis, PCA Principal Component Analysis, G-RBF, Gaussian Radial Basis Functions, SSM Statistical Shape Model.

fracture, who received a similar robot-assisted surgical intervention. The skeletal models for the two patients were processed using the CT-bone auto-segmentation tool in Mimics software, involving the identification of critical skeletal regions, setting appropriate bone greyscale thresholds, and generating STL files for distinct bone sections via the Calculate Part tool. Since the clinical CT scans, which included the pelvic region and part of the femur, only captured partial femur images, a complete femur model scanned from a synthetic sawbone femur[35] was substituted using the ICP registration method to determine the relative positions of the lower limb and pelvic muscles[36]. The resultant STL files, including models of the affected and healthy pelvic sides, the affected femur, and the spinal structure, were imported into SolidWorks for assembly with the surgical gripping device. The skeletal model reconstruction process is illustrated in Fig. 3A.

Subsequently, the SMAG method was employed to autonomously generate muscle models for the patients. In the SMAG method, muscle attachment points are determined in two stages. First, the muscle attachment points on the femur are identified using the ICP method. By marking these points on a complete sawbone femur model and transforming it to align with the patient's femur, the corresponding attachment points on the patient's femur are obtained (Fig. 3B). Second, the muscle attachment points on the pelvis are adaptively adjusted by marking them on the SSM template. The SSM template was developed from ilium and sacrum data of 40 open-source pelvic datasets, as detailed in the Methods section. Iterative calculations on the SSM template yield transformation parameters ($\hat{\boldsymbol{b}}_{\mathbf{ssm}}$) that adapt the SSM template to the patient's pelvic model (Fig. 3C). These muscle attachment points are then mapped to the corresponding positions on the adjusted patient-specific pelvic model. The specific coordinates of muscles and ligaments on the pelvis and femur are detailed in Supplementary Tables 2–7. Reconstructing each patient's muscle model involves identifying 70 sets of muscle and ligament attachment points. Using the SMAG method, automated reconstruction of the patient's muscle model takes just 29.8 s, significantly enhancing efficiency and precision of muscle model reconstruction.

Finally, we utilized the OpenSim platform API tools to integrate the patient's skeletal and muscle models and conduct a mechanical analysis of the reconstructed musculoskeletal model (Fig. 3D). OpenSim is an exemplary platform for detailed biomechanical analyses and parameterization, incorporating a sophisticated muscle framework model[37–39]. The reconstructed model includes the fractured and healthy pelvis, spine, surgical device (gripper), and femur. Movements are defined by coordinate system changes (joints). The healthy pelvis and L4–L5 vertebrae are connected to the global coordinate system via Weld joints. A free joint attaches the gripper to the global coordinate system, while another Weld joint links the fractured pelvis to the gripper, enabling prescribed motion. A ball joint connects the femur to the fractured pelvis. For the mechanical analysis, we used the Millard2012EquilibriumMuscle model in OpenSim to define the muscle's mathematical relationships[40]. Muscle parameters, including maximum isometric force, optimal fiber length, pennation angle, and muscle slack length, were based on the Gait2392 model (Supplementary Table 8)[41]. The muscle model had a damping coefficient of 0.01 and excluded tendon yield properties. Ligaments were reconstructed using OpenSim's PathSpring tool, with parameters detailed in Supplementary Table 9. Six coordinate actuators, each calibrated for an optimal force output of 1 N, were integrated at the gripper's terminal end to provide precise force and torque feedback for biomechanical analysis and simulation.

Statistics and reproducibility

This study utilized a cohort of 10 patients with pelvic fractures for biomechanical validation, conducted in accordance with the ethical protocol approved by the Institutional Review Board of Jishuitan Hospital (Approval No. 20210901). The statistical shape model (SSM) was constructed based on 40 open-source pelvic datasets, the acquisition and anatomical validity of which have been previously established and comprehensively validated in our earlier work[25]. The anatomical fidelity of patient-specific SSM adaptations was mathematically ensured through: (1) landmark correspondence optimization via Euclidean distance minimization, and (2) physiological deformation bounds defined by Eq. 5.

Model validation was performed by comparing simulation outputs against intraoperative measurements from representative patients, with methodological details provided in the Validation subsection (Section "Validation of Musculoskeletal Models Using Recorded Force Data from Clinical Surgery"). To evaluate the robustness and clinical utility of the framework, each patient-specific model was used to simulate five distinct reduction paths under consistent initial conditions. The variation in predicted reduction forces across these paths was quantitatively compared to assess the model's sensitivity to surgical approach, thereby providing a measure of procedural reproducibility.

The full dataset of 40 open-source pelves and deidentified clinical images is available upon reasonable request[28]. Complete simulation protocols and OpenSim configuration files (e.g., Kinematics_Tracking_Tasks.xml) are available in the public repository[42]. Reconstruction accuracy was quantified using Euclidean distance between predicted and ground-truth landmarks. All statistical and geometric computations were performed using Python (v3.9) with SciPy and NumPy libraries.

Results

Data collection from clinical surgeries and dynamic analysis of musculoskeletal models

Data acquisition was conducted in a sterile surgical environment (Fig. 4A). The surgical team performed pelvic reduction procedures using a UR16e robotic system equipped with: Integrated bedside passive-arm stabilizer, NDI optical tracking system, and ATI 6-axis force measurement apparatus.

The fractured pelvis is rigidly attached to a UR16e robot through a gripper and reduced under NDI optical navigation guidance. The healthy pelvis is stabilized with a bedside passive arm. The NDI optical tracking system (Northern Digital Inc.) recorded spatial trajectories of bone fragments at 40 Hz. The ATI Mini45 6-axis F/T sensor (SN: MCE-45623) was rigidly mounted between the UR16e robotic end-effector and pelvic reduction gripper. Force/torque data were continuously acquired at 20 Hz via the UR16e's Real-Time Data Exchange (RTDE) interface. Due to the different sampling frequencies of the NDI optical system (40 Hz) and the robotic RTDE interface (20 Hz), all data streams were aligned during post-processing using a unified timestamp generated by the host control computer. Synchronization was achieved by identifying a common start event (e.g., the initiation of the reduction maneuver) across data streams, and the temporal alignment was verified by checking the consistency of key time points throughout the procedure. This method ensured temporal accuracy without risk of cumulative drift.

Figure 4B delineates the prerequisite datasets for subsequent biomechanical analysis, comprising spatial trajectory files recorded by the NDI optical tracking system (40 Hz sampling) and constraints to simulate fracture reduction (hip joint movement). Output parameters encompass muscle forces and the forces and torques required for the reduction, computed using the Computational Muscle Control (CMC) tool in OpenSim[43]. The time step for CMC computations was set to a minimum of 0.03 s. The activation level for all muscle actuators was uniformly set at 0.05, considering the use of muscle relaxants during surgery to maintain muscle activation levels within a stable range (0.02–0.05)[44].

Figure 4C, D illustrate pelvic spatial displacement and posture data for Patient 1 during reduction surgery. The robotic-assisted reduction for this patient lasted 2 min and 14 s (15:42:54–15:45:08 on August 30, 2021), with force data normalized to a 0–140 s interval (5322 data points). Correspondingly, Fig. 4E, F present the same types of data for Patient 2, whose procedure duration was 4 min and 35 s (13:23:12–13:27:47 on June 27, 2022), normalized to 0–276 s (5520 data points). Analysis showed that the spatial poses of the bone fragments initially changed significantly before stabilizing, termed the Reduction phase. For Patient 1, this phase lasted from 0 to 77 s and for Patient 2, from 0 to 125 s. The subsequent phase, termed the Jittering process, involves oscillation around consistent values. The displacement and posture data from the Reduction phase will serve as target motion trajectories for biomechanical analysis in the musculoskeletal model.

Validation of musculoskeletal models using recorded force data from clinical surgery

Since direct intraoperative muscle force measurement remains clinically infeasible, we utilize the readily measurable robotic reduction forces as validation benchmarks. This strategy is particularly appropriate for our force-line modeling approach, where muscle attachment points are determined through surgeon-identified centroids of anatomical zones—a method that

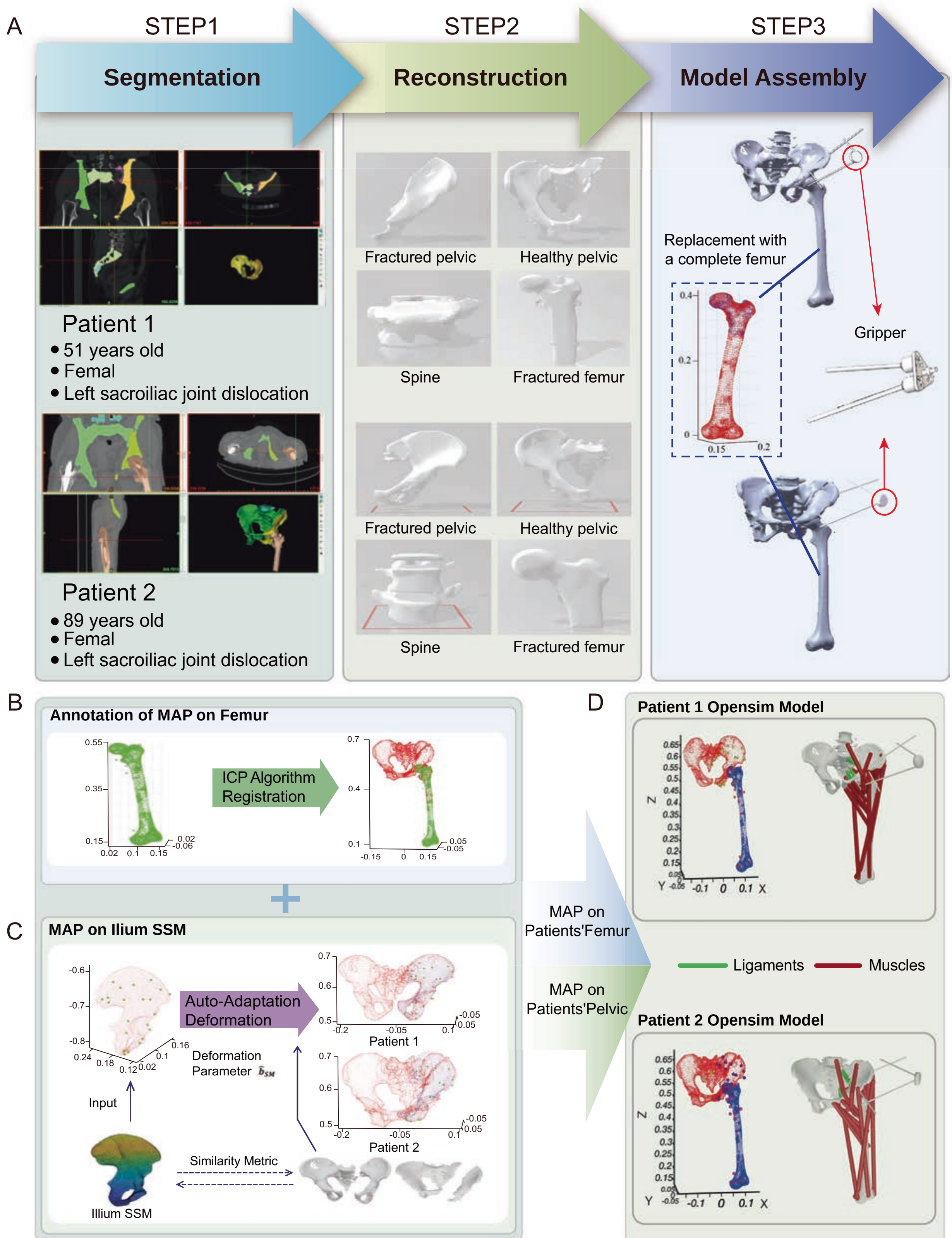

Fig. 3 | Workflow of patient-specific musculoskeletal modeling using the SMAG framework. A Reconstruction process of the patient's skeletal model. **B** SMAG method for muscle model reconstruction: Identifying femoral muscle attachment points using ICP rigid transformation. **C** SMAG method for muscle model reconstruction: Determining pelvic muscle attachment points using SSM adaptive transformation. **D** Integration of the patient's skeletal and muscle models in OpenSim for mechanical analysis. Abbreviations: SSM Statistical Shape Model, MAP Muscle Attachment Point.

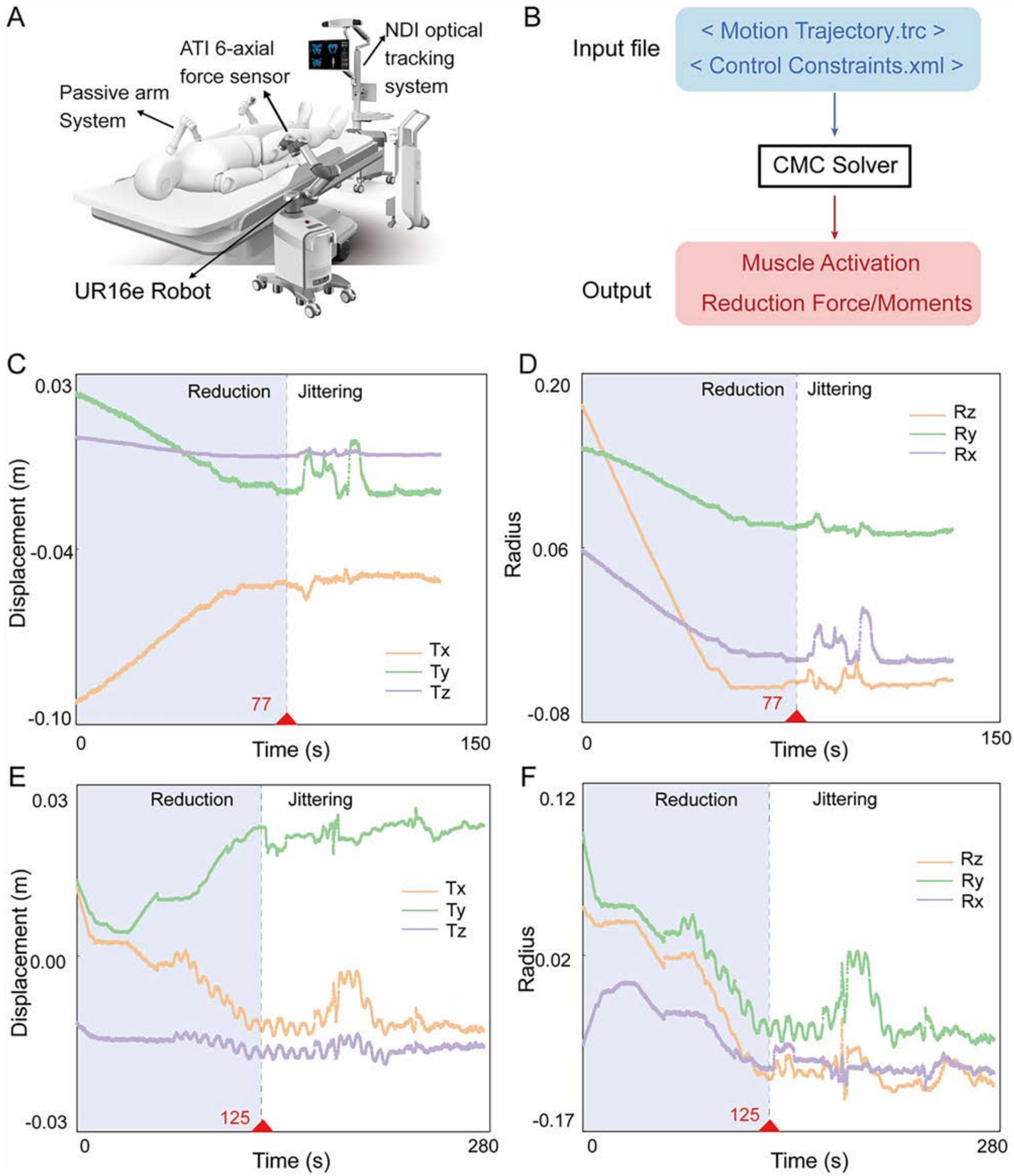

Fig. 4 | Clinical Data Acquisition and Experimental Setup. A Schematic of the robotic system for pelvic fracture reduction. **B** Biomechanical analysis workflow using the CMC tool in OpenSim. Inputs: motion trajectory, control constraints. Outputs: muscle activation, reduction forces/moments. **C**–**F** Pelvic displacement and posture data during reduction surgery. **C**, **D** Displacement (Tx, Ty, Tz) and Rotation (Rx, Ry, Rz) for Patient 1, Reduction phase (0–77 s). **E**, **F** Displacement (Tx, Ty, Tz) and Rotation (Rx, Ry, Rz) for Patient 2, Reduction phase (0–125 s). Abbreviations: UR16e collaborative robot, ATI force sensor, NDI optical tracking system, CMC computed muscle control.

inherently prioritizes functional representation over micron-level morphological precision. The anatomical accuracy of our patient-specific SSM adaptations is mathematically guaranteed through two fundamental constraints: Landmark correspondence optimization via Euclidean distance minimization and Physiological deformation bounds, as defined in Eq. 5.

Figure 5 presents pelvic reduction force and moment data for Patient 1 (5A-5D) and Patient 2 (5E-5H). Similar to displacement and posture data, the forces and moments initially fluctuate before stabilizing due to dynamic changes in bone positions, soft tissues, and the sensitivity of the force sensors. We recorded the times at which maximum output force (5 A, 5E) and

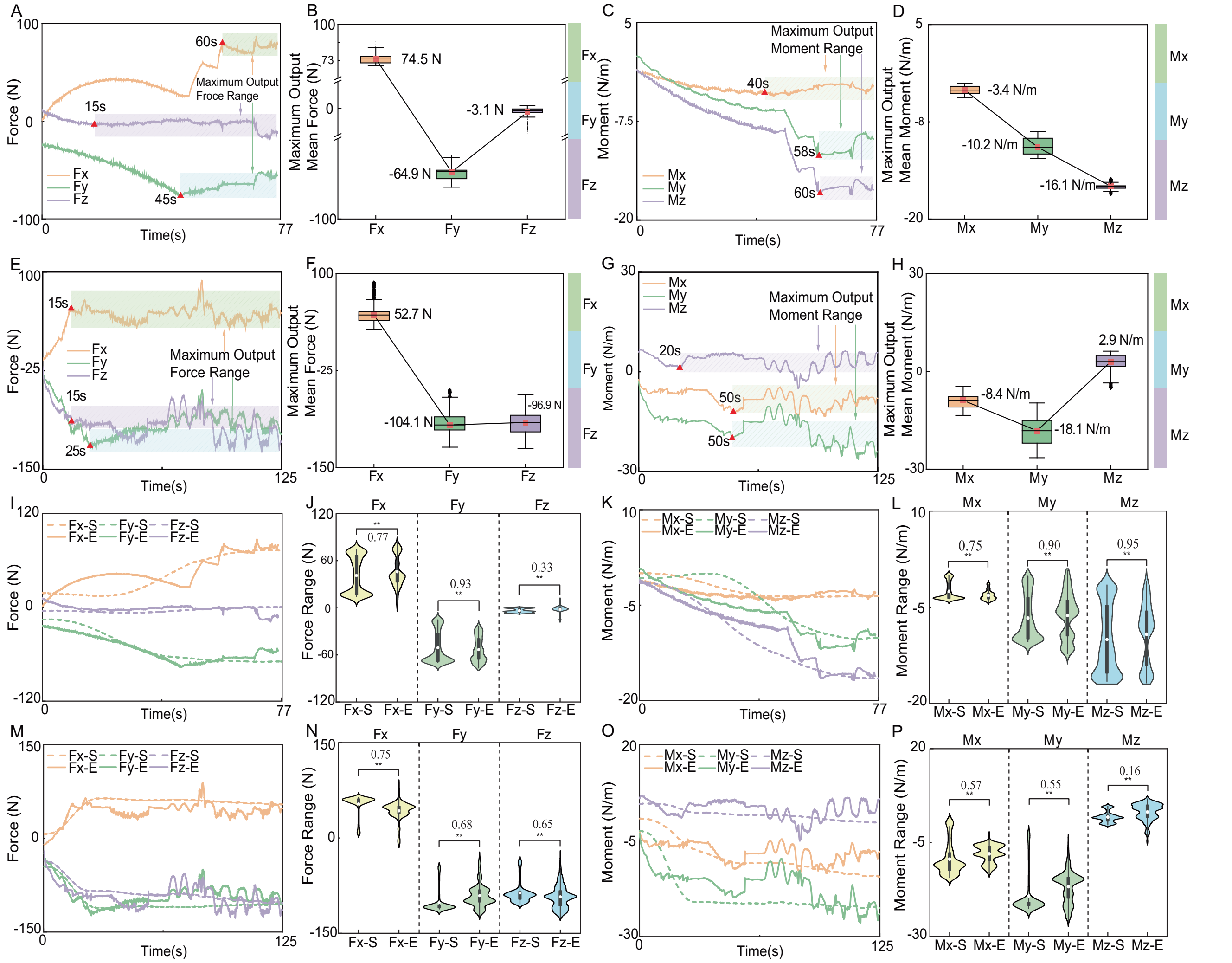

Fig. 5 | Comparison of Clinical and Simulation Data for Pelvic Reduction Forces and Moments. A, **B** Force data and maximum output mean force values for Patient 1. **C**, **D** Moment data and maximum output mean moment values for Patient 1; **E**, **F** Force data and maximum output mean force values for Patient 2. **G**, **H** Moment data and maximum output mean moment values for Patient 2; **I**, **K** Comparison of force and moment data from the SMAG model and clinical data for Patient 1. **J**, **L** Statistical significance of Fx, Fy, Fz and Mx, My, Mz data for Patient 1; **M**, **O** Comparison of force and moment data from the SMAG model and clinical data for Patient 2. **N**, **P** Statistical significance of Fx, Fy, Fz, and Mx, My, Mz data for Patient 2. Error bars in the box plots represent standard deviation. The sample sizes (N values) used to calculate the maximum output force and moment are as follows: For Patient 1, $N = 320$ for Fx, $N = 620$ for Fy, $N = 1220$ for Fz, $N = 720$ for Mx, $N = 360$ for My, and $N = 320$ for Mz;For Patient 2, $N = 1220$ for Fx, $N = 1020$ for Fy, $N = 1220$ for Fz, $N = 520$ for Mx, $N = 520$ for My, and $N = 1120$ for Mz.

output moment (5 C, 5 G) ranges began, as well as the maximum output mean force (5B, 5 F) and output mean moment (5D, 5H) values. Detailed numerical values are provided in Supplementary Tables 10–11. The complete set of raw clinical and simulated data for both patients has been made publicly available in the designated database[42].

When calculating muscle forces during pelvic reduction, the CMC tool uses static optimization and proportional-integral methods, resulting in stable force and moment outputs. To better mimic the temporal changes observed during the actual procedure, we adjusted the timing functions of force and moment signals based on the clinical data's maximum output times.

Figure 5I–L compare biomechanical data obtained using the SMAG modeling method with clinical data for Patient 1, while Fig. 5M–P present the comparison for Patient 2. Our analysis employs Pearson correlation to evaluate temporal similarity in force/torque waveforms and spatial distribution consistency across positions. To preserve clinical authenticity, we maintain raw intraoperative force data without filtering. By driving both clinical and simulated systems with identical NDI-recorded reduction trajectories our validation paradigm inherently cancels motion artifacts and sensor noise while isolating model prediction accuracy from physiological variance.

Force (Fig. 5I, M) and moment data (Fig. 5K, O) obtained using the SMAG method for both patients showed consistent trends with clinical data. A non-parametric test for two independent samples was used to determine significant differences in the distribution between clinical and simulation data. Figures 5J and 5N display the significance of Fx, Fy, and Fz data, while Fig. 5L, P show the significance of Mx, My, and Mz data. The results significantly correlate with the clinical data for both patients, validating the effectiveness of the SMAG method for patient-specific modeling. Detailed numerical values are provided in Supplementary TableS 12–13.

Accuracy and efficiency of SMAG, Standard Scaling and manual annotation method

We compared the SMAG method's modeling efficiency with manual annotation and its accuracy with the standard scaling method. The comparison included overall model reconstruction time and the error between modeled and clinical reduction forces and moments. The generic model used in the scaling method was the Gait 2392 lower limb model, with scaling

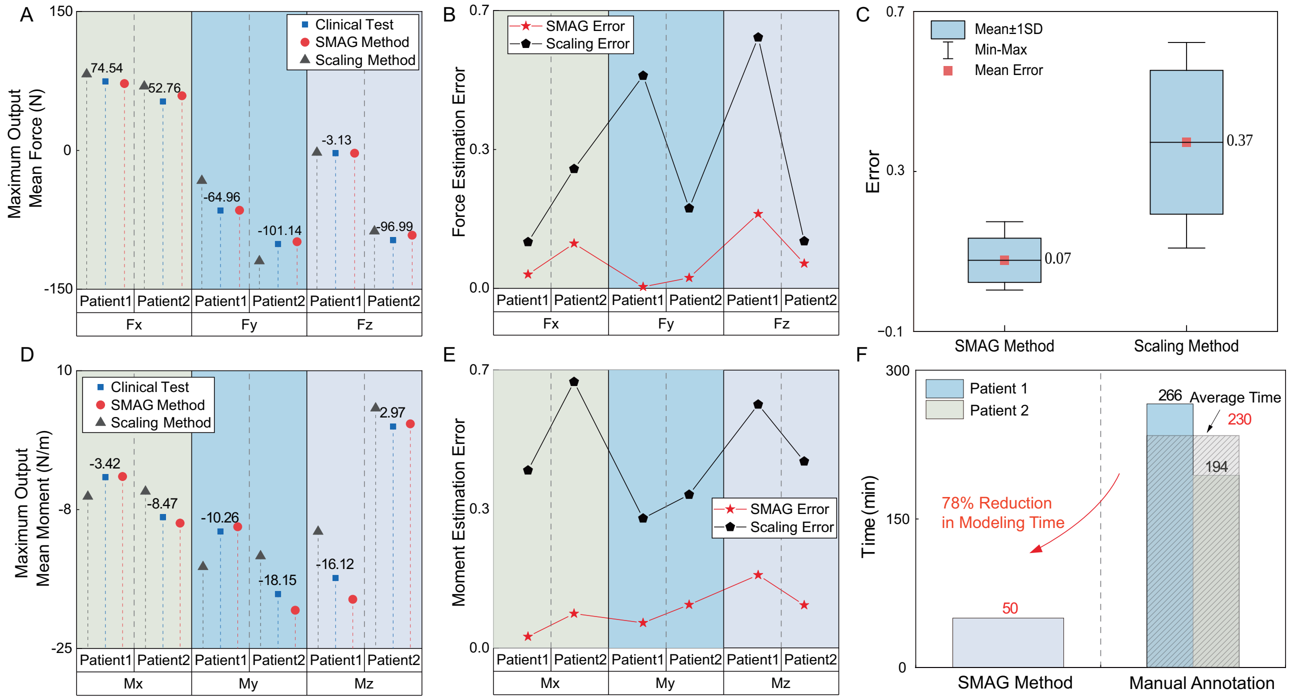

Fig. 6 | Comparison of SMAG-generated forces/moments with clinical data and conventional methods. A, **D** Comparison of forces and moments calculated using SMAG and generic scaling methods with clinical data for two patients. **B**, **E** Errors in force and moment calculations between clinical data and those obtained using SMAG and scaling methods. **C** Average errors for force and moment calculations using SMAG (0.07) and scaling method (0.37). **F** Comparison of time required for constructing patient-specific musculoskeletal models using the SMAG method versus manual annotation. Abbreviations: SMAG Statistical Musculoskeletal Automatic Generator.

ratios determined by measuring the length, width, and height of the healthy iliac wing. Detailed scaling methodologies can be found on the OpenSim website[45].

Figure 6 compares pelvic reduction forces and moments calculated using the SMAG method and the generic scaling method with clinical data for two patients. In Fig. 6A–D, blue boxes represent the actual forces and moments recorded during surgeries. Figure 6B shows the error in force calculations, while Fig. 6E shows the error in moment calculations for both methods. The errors in forces and moments calculated by the SMAG method (red pentagrams) are significantly lower than those from the generic scaling method (black pentagons). Figure 6C displays the average errors for forces and moments, with the SMAG method achieving an average error of 7.7% compared to 37.2% for the scaling method. Detailed numerical values are provided in Supplementary Tables 10–11.

We evaluated the time required for constructing patient-specific musculoskeletal models using the SMAG method (Fig. 6F). The process includes skeletal model reconstruction, which takes approximately 30 min and involves automated bone segmentation, fine-tuning, and generating STL files. Muscle model reconstruction requires about 10 min for adaptive SSM matching and generating muscle attachment points. Constructing the musculoskeletal model in OpenSim takes an additional 10 min. Thus, the total time for the entire process is approximately 50 min. In contrast, manual annotation methods significantly increase the time required. Ignoring incidental factors like computer speed or interruptions, manually annotating 28 force line elements (23 muscle groups and 5 ligaments) with 60 intermediate points took 4 h and 26 min for Patient 1 and 3 h and 14 min for Patient 2, averaging 230 min. Figure 6F compares the average modeling times using manual annotation versus the SMAG method, showing a 78% reduction in modeling time with the SMAG method. These results indicate that the SMAG method significantly enhances both the accuracy and efficiency of constructing patient-specific musculoskeletal models.

Extended validation of the SMAG method with additional clinical data

To further validate the SMAG method, we compared it with additional clinical data from 8 cases of unilateral pelvic fracture reductions, including 4 left iliac dislocations and 4 right iliac dislocations (Fig. 7A, B). Using the SMAG method, personalized musculoskeletal models were reconstructed in under 1 h on average. Figure 7C–H illustrate the forces required for reduction, calculated using these patient-specific models along the recorded clinical reduction paths. Figure 7C shows the comparison of reduction force Fx between the SMAG method and clinical records, with Fig. 7D displaying the corresponding errors and error rates. Similarly, Fig. 7E, G present comparisons for reduction forces Fy and Fz, while Fig. 7F, H show their respective errors and error rates. Detailed numerical values are provided in Supplementary Table 14.

Analysis of the results showed that the absolute errors between the SMAG method and clinical trial data for reduction forces Fx, Fy, and Fz were all less than 10 N, with error rates generally around 10%. This 10 N threshold represents a clinically acceptable margin, as pelvic fracture reduction typically applies 15–25 N traction forces while maintaining neurovascular safety limits below 10 N. It is important to note that the high percentage errors predominantly occur at low absolute forces of less than 20 N, where minor variations magnify the percentages. For instance, the 64.3% error for Patient 7's Fz force corresponds to a mere 1.3 N deviation (−2.0 N vs. −3.3 N). Similarly, Patient 5's Fx error of 27.5% represents just a 5.03 N absolute difference (−18.2 N vs. −13.2 N).

Overall, the average error rate across Fx, Fy, and Fz for the 8 patients was 13.8%. In surgical practice, resultant force vectors—not isolated components—determine biomechanical risk, as exemplified by Patient 7: while its Fz component showed 64.3% error (1.3 N deviation), the resultant force error measured just 7.4 N (14.3%), well below neurovascular injury thresholds (<10 N). This vector-sum approach inherently reduces net error rates by compensating for opposing directional inaccuracies.

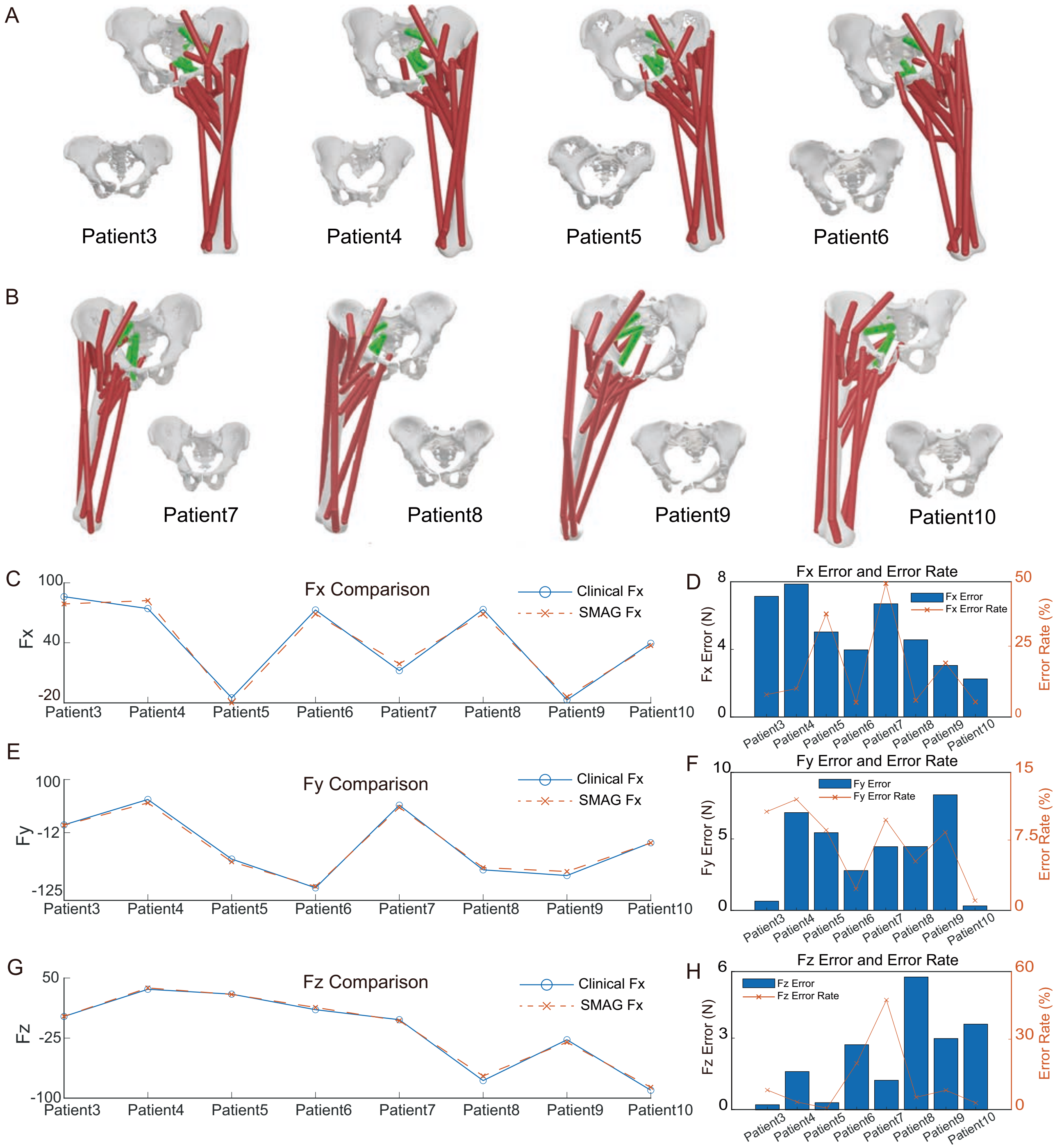

Fig. 7 | Validation of patient-specific SMAG models across multiple fracture cases using clinical reduction forces. A, B Personalized musculoskeletal models using the SMAG method for eight patients with unilateral pelvic fractures. **A** Left iliac dislocation reductions. **B** Right iliac dislocation reductions. Red lines represent muscles, and green lines represent ligaments. **C, D** Comparison of reduction force Fx between clinical data and SMAG method. **C** Line plot of Fx data. **D** Error and error rate. **E, F** Comparison of reduction force Fy. **E** Line plot of Fy data. **F** Error and error rate. **G, H** Comparison of reduction force Fz. **G** Line plot of Fz data. **H** Error and error rate.

The application in preoperative planning for pelvic surgery

Constructing patient-specific musculoskeletal models allows for mechanical analysis of pre-surgical plans, providing decision support in clinical applications. Based on the clinical reduction path (Path 1), we developed four additional reduction paths (Path 2 to Path 5) for Patients 1 and 2 (Fig. 8A, B). Each path maintains the same initial and target poses. The strategies are described as follows: Path 1 represents the actual surgical trajectory and is marked by a blue dot. Path 2, indicated by a red cross, involves sequential translations and rotations along the X, Y, and Z axes. Path 3, shown with a yellow diamond, uses a uniform interpolation of translations and rotations

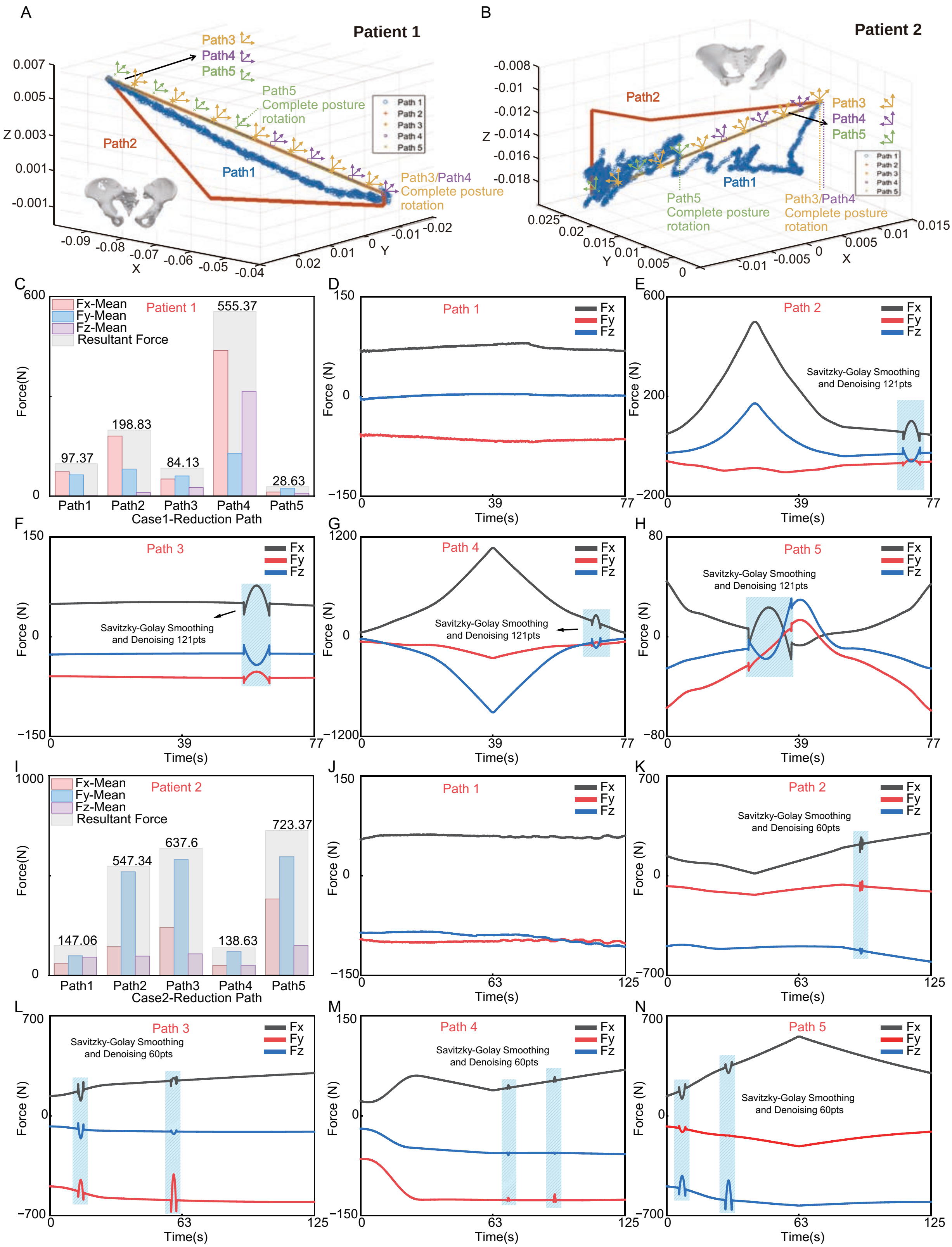

Fig. 8 | Evaluation of surgical reduction paths and associated reduction force profiles. 3D visualization of five reduction paths (Path 1 to Path 5) for Patient 1 (**A**) and Patient 2 (**B**). Reduction force comparison for Patient 1 (**C**) and Patient 2 (**I**) across different paths. Detailed numerical values are provided in Supplementary Tables 15–16. **D**–**H** Reduction force curves for Patient 1 using Paths 1 to 5. Path 1 maintains stability without singular values, while Paths 2 to 5 exhibit fluctuations, smoothed using Savitzky-Golay filtering. **J**–**N** Reduction force curves for Patient 2 using Paths 1 to 5.

across all six axes (X, Y, Z, Rx, Ry, Rz). Path 4, denoted by a purple square, applies translations along the X, Y, and Z axes first, followed by rotations around Rx, Ry, and Rz. Finally, Path 5, displayed by a cyan cross, performs the reverse sequence, executing rotations first, followed by translations.

Figure 8C, D display the specific reduction forces for Patient 1 and Patient 2 during the reduction process using the musculoskeletal model simulation. Figure 8E–H, J–N show the variation in reduction forces for the five different paths for Patient 1 and Patient 2, respectively. The smoothness of the reduction force curves indicates that the clinically recorded path (Path 1) maintains greater stability throughout the simulation without singular values. This stability is due to the robotic arm pausing when encountering extreme forces and recalibrating to find a smoother trajectory. In contrast, the four artificially created paths (Paths 2–5) include extreme positions that lead to singular values in the calculations. Savitzky-Golay filtering is employed to smooth out these singular values, enhancing the continuity of the reduction force curves.

Analysis of the reduction forces shown in Fig. 8C, D highlights the mechanical advantages of different reduction strategies. The reduction forces significantly vary with the strategy employed. For Patient 1, the actual clinical reduction path (Path 1) displays relatively lower resultant forces, indicating that the robotic arm adaptively optimized its mechanics to minimize force while staying within load limits. However, Path 5 showed an even lower force (28.6 N) compared to Path 1 (97.3 N), suggesting further optimization potential. For Patient 2, the optimal reduction path was Path 4, which involves initial X-Y-Z translations followed by Rx-Ry-Rz rotations. Paths 3 and 5, which were optimal for Patient 1, did not yield similar results for Patient 2, underscoring the necessity for customized reduction strategies tailored to individual patients.

Analysis of muscle force components and vector direction for optimizing robotic-assisted pelvic fracture reduction

The clinical value of personalized musculoskeletal models is highly significant in surgery, as they accurately predict the mechanical distribution of key muscles and ligaments during procedures. This enables surgeons to identify and adjust high-stress tissues, reducing the risk of intraoperative injuries. Figure 9A, D show the changes in major ligament forces during pelvic reduction for Patients 1 and 2, while Fig. 9B, E display the dynamic changes in forces across 22 muscle groups. This visualization provides critical insights into how different reduction paths affect muscle loads, aiding in the evaluation and optimization of surgical strategies. Based on this analysis, Fig. 9I presents the distribution of key muscle and ligament forces for five reduction paths in both patients, using a sunburst chart. This visualization identifies major resistance-producing muscles and their anatomical locations in each path, offering surgeons a clear reference to adjust surgical techniques or release specific muscles, thereby minimizing surgical damage. Detailed numerical values are provided in Supplementary Table 17.

For robot-assisted surgeries, biomechanical assessments of reduction paths clarify the force dynamics on bones and soft tissues, offering precise guidance to ensure applied forces remain within safe thresholds. Figure 9G, H illustrate the changes in resultant muscle force vectors during reduction. From left to right (i-iii): (i) individual muscle force directions and magnitudes, (ii) resultant force vectors calculated at the center of mass, and (iii) the angle between resultant force vectors and anatomical displacement vectors. This angle reflects the deviation between mechanical and anatomical reductions, with mechanical reduction ensuring procedural fluidity and anatomical reduction guaranteeing final alignment quality.

This analysis is critical for improving robotic efficiency. For example, UR-series robotic arms exhibit higher operational force along the Y-axis than the X-axis. Biomechanical modeling can identify the direction of maximum resistance, allowing alignment of the Y-axis for optimized output and positioning. Additionally, when reduction forces exceed safe thresholds, the tangential component of the resultant vector can indicate paths of least resistance, improving robotic efficiency. Finally, personalized models predict force requirements at each step of reduction, providing a biomechanical basis for safe and effective path planning. This optimizes reduction strategies, improves surgical efficiency, and reduces patient risks.

Discussion

The present study demonstrates that quantitative biomechanical analysis plays an instrumental role in pelvic fracture reduction, transforming subjective surgical experience into objective, data-driven guidance. By characterizing force distributions and dynamic changes during reduction, our approach provides a reproducible framework that is particularly beneficial for surgical training, standardization of clinical workflows, and the enhancement of robotic-assisted surgery. The integration of biomechanical assessments enables surgeons to preoperatively optimize reduction strategies, minimize operative time, and mitigate risks associated with excessive force or repeated reduction attempts—addressing critical challenges highlighted in prior studies[11,15,46].

A significant barrier to the widespread adoption of biomechanical guidance in surgery has been the difficulty in generating accurate and efficient patient-specific musculoskeletal models. Traditional methods, though anatomically informative, are hampered by labor-intensive processes and limited precision, particularly in capturing real-time mechanical interactions[15,16]. Manual annotation of muscle attachments remains time-consuming and operator-dependent, restricting clinical utility[17,47]. While MRI-based models improve geometric accuracy, they struggle with automated segmentation and computational efficiency, especially in anatomically complex regions like the pelvis[47]. In contrast, force-line models provide a favorable balance between speed and accuracy, as confirmed by Jensen et al., who reported errors as low as 1–12% compared to more complex geometric methods[20].

Our proposed SMAG framework overcomes these limitations through the application of Statistical Shape Models, enabling automated, rapid, and precise generation of patient-specific musculoskeletal models[48,49]. By leveraging population-based anatomical variations, SMAG significantly reduces manual intervention and improves both the efficiency and accuracy of model reconstruction. This method aligns with growing emphasis on incorporating musculoskeletal constraints into orthopedic robotics, as observed in recent literature[49–51]. The results indicate a 78% improvement in modeling efficiency and a substantial reduction in reconstruction[52,53] errors —from 41.3% and 33.2% to 7.7% and 5.4%—confirming the robustness and clinical applicability of SMAG across multiple validation cases.

Notably, the method also supports real-time biomechanical feedback within robotic systems, allowing adaptive surgical execution and enhanced operational safety. This is particularly important given the force limitations inherent in many surgical robotic systems (e.g., the 160 N safety threshold), where exceeding mechanical limits may lead to system halt and procedural failure[9,10,46]. SMAG's ability to preoperatively simulate and evaluate reduction pathways offers a viable solution to avoid intraoperative interruptions and improve surgical fluency.

Several limitations warrant acknowledgment. Although SMAG excels in anatomical reconstruction and static force prediction, it currently relies on simplified force-line models for muscle representation. This approach, while efficient, does not fully capture the dynamic three-dimensional behavior of muscles and soft tissues under varying loading conditions[17,47]. Furthermore, as observed in our validation, moments around the Z-axis (Mz) exhibited relatively low correlation ($R^2 = 0.16$), which can be attributed to the biomechanical profile of sacroiliac joint dislocations where reduction is primarily translational with minimal rotational component. Despite the low correlation, the model correctly predicted the near-zero magnitude of Mz, reflecting clinical observations. Additionally, while SSM effectively represents bony anatomy, modeling the nonlinear mechanical behavior of soft tissues remains challenging[16,17].

Future research should focus on enhancing the dynamic fidelity of musculoskeletal models, incorporating real-time feedback mechanisms, and expanding the demographic diversity of underlying datasets to improve generalizability. Algorithmic optimizations are needed to better account for soft tissue mechanics and singularity avoidance in motion planning. The

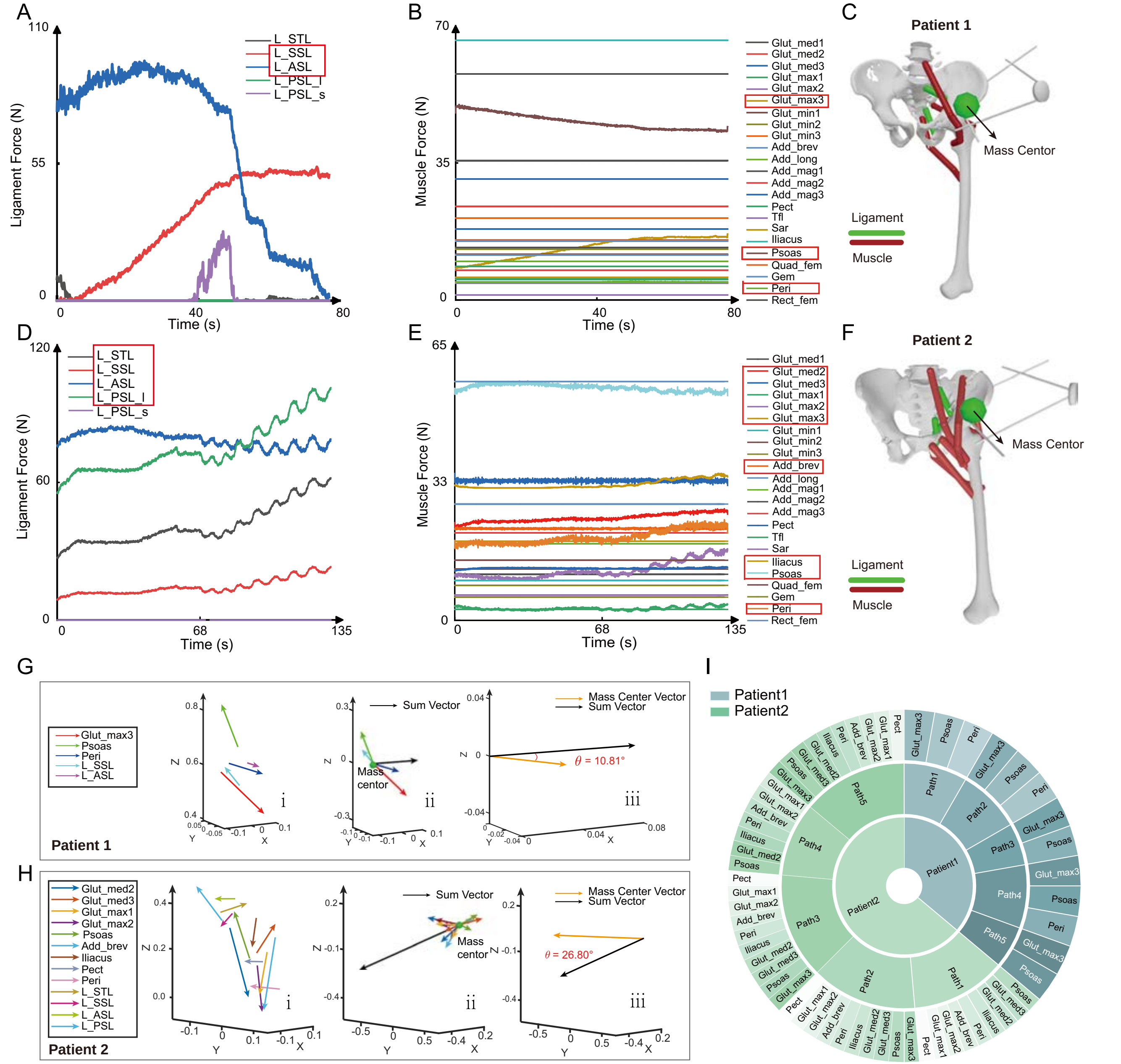

Fig. 9 | Biomechanical analysis and optimization of reduction pathways using personalized musculoskeletal models. A, **D** Ligament force variations during pelvic reduction for Patient 1 and Patient 2; **B**, **E** Muscle force changes for 22 key muscles during the reduction process; **C**, **F** Mass center positions and force directions for Patients 1 and 2; **G**, **H** Resultant force vector analysis: (i) Key muscleand ligament force vector directions; (ii) Combined resultant force vector directions for muscle groups; (iii) Angle between the resultant force vector and the anatomical mass center vector, showing alignment differences (10.8° for Patient 1, 26.8° for Patient 2), highlighting the balance between mechanical and anatomical reduction; **I** Sunburst diagram visualizing ligament and muscle forces across five reduction pathways, providing insights for preoperative planning by identifying key load-bearing tissues. Abbreviations: Glut_med Gluteus medius, Glut_max Gluteus maximus, Glut_min Gluteus minimus, Add_brev Adductor brevis, Add_long Adductor longus, Add_mag Adductor magnus, Pect Pectineus, TFL Tensor fasciae latae, Sar Sartorius, Iliacus Iliacus muscle, Quad_fem Quadratus femoris, Gem Gemellus, Piri Piriformis, Rect_fem Rectus femoris, L_djrd, Sacrospinous ligament, L_djjrd Sacrotuberous ligament, L_dqqrd Anterior sacroiliac ligament, L_dqhrd_l Long posterior sacroiliac ligament, L_dqhrd_s Short posterior sacroiliac ligament.

integration of multi-scale modeling—from macroscopic anatomy to microscopic tissue properties—may further bridge the gap between computational efficiency and biological accuracy.

Conclusion

In summary, the SMAG framework represents a meaningful advance in patient-specific biomechanical modeling for pelvic fracture surgery. By automating the generation of musculoskeletal models with high efficiency and accuracy, SMAG facilitates data-driven surgical planning and execution. Its integration with robotic systems promises to enhance precision, safety, and adaptability in the operating room. While challenges remain in real-time soft tissue modeling and dynamic force prediction, this study lays a foundation for future developments in intelligent and personalized orthopedic surgery.

Ethical approval

This study was conducted in accordance with the ethical standards of the Institutional Review Board of Beijing Jishuitan Hospital (Approval No. 202109-01) and the 1964 Helsinki Declaration. For the clinical data, written informed consent was obtained from all individual participants.

For the public dataset (PelvisAtlas), its use constituted secondary analysis of de-identified data, which is considered non-human subjects research. All patient data from both sources were anonymized to protect privacy.

Data availability

The datasets generated and analyzed during this study include:1.Case1_pelvicreduction_model: Skeletal model of Patient 1 with reduction trajectory data and muscle attachment point annotations. 2.Case2_pelvicreduction_model: Skeletal model of Patient 2 with reduction trajectory data and muscle attachment point annotations. 3.SSMfitting_Case1_and_Case2: Data files for Statistical Shape Model (SSM) fitting and template-to-patient adaptation. 4. Complete set of raw clinical and simulated data for both patients. These datasets have been deposited in the Mendeley Data repository[42] and are publicly available at: https://data.mendeley.com/datasets/6m97r8p44s/153. Additionally, we utilized the following publicly accessible dataset for method development: Open-Source Pelvis Atlas[29] (I-STAR Lab, Johns Hopkins University): A repository of 40 pelvis CT segmentations and statistical shape models (SSM). Access: https://github.com/I-STAR/PelvisAtlas The atlas derives from 40 CT images of the pelvis adapted from The Cancer Imaging Archive (TCIA) CT Lymph Node database[28]. For the original CT images, please go to the original database: Access: https://wiki.cancerimagingarchive.net/display/Public/CT+Lymph+Nodes

Code availability

The custom code developed for this study is publicly available in the same Mendeley Data repository: 1. SSM-Based Muscle Attachment Mapping Code for adaptive annotation of patient-specific muscle attachment points. 2. OpenSim Workflow Scripts for reconstructing patient-specific musculoskeletal models and simulating biomechanical analyses. Access the code via the public repository[42] at: https://data.mendeley.com/datasets/6m97r8p44s/153.

Received: 20 January 2025; Accepted: 22 October 2025;
Published online: 15 November 2025

References

1. Burgess, A. R. E. et al. Pelvic ring disruptions: effective classification system and treatment protocols. *J. Trauma* **30**, 848–856 (1990).
2. Matta, J. M. et al. 3rd Internal fixation of unstable pelvic ring injuries. *Clin. Orthop. Relat. Res.* **329**, 129–140 (1996).
3. Blum, L. H. et al. C Vertical shear pelvic injury: evaluation, management, and fixation strategies. *Int. Orthop* **42**, 2663–2674 (2018).
4. Liu, J. et al. Experimental and finite element analysis studies of a reduction-force reducing traction method for pelvic fracture surgeries. *Med. Novel Technol. Devices* **13**, 100101 (2022).
5. Garcia, M. et al. Severe pelvic fracture in the elderly: high morbidity, mortality, and resource utilization. *Am. Surg.* **86**, 1401–1406 (2020).
6. Elabjer, E., Nikolic, V., Matejcic, A., Stancic, M. & Kuzmanovic Elabjer, B. Analysis of muscle forces acting on fragments in pelvic fractures. *Coll. Antropol.* **33**, 1095–1101 (2009).
7. Pielak, T. et al. The Association between BMI, Days Spent in Hospital, Blood Loss, Surgery Time and Polytrauma Pelvic Fracture—A Retrospective Analysis of 76 Patients. *Appl. Sci.* **13**, 10546 (2023).
8. Lundin, N. & Enocson, A. Complications after surgical treatment of pelvic fractures: a five-year follow-up of 194 patients. *Eur. J. Orthop. Surg. Traumatol.* **33**, 877–882 (2023).
9. Zhao, C. et al. Intelligent robot-assisted minimally invasive reduction system for reduction of unstable pelvic fractures. *Injury* **54**, 604–614 (2023).
10. Liu, J. et al. Biomechanical analysis of pelvic holding pathways and strategies for use of the steinmann pin in pelvic fracture reduction. *Comput. Biol. Med.* **152**, 106310 (2023).
11. Ge, Y., Zhao, C., Wang, Y. & Wu, X. Robot-assisted autonomous reduction of a displaced pelvic fracture: a case report and brief literature Review. *J. Clin. Med.* **11**, 1598 (2022).
12. Han, R. et al. Fracture reduction planning and guidance in orthopaedic trauma surgery via multi-body image registration. *Med. Image Anal.* **68**, 101917 (2021).
13. Fernandez, J. et al. Multiscale musculoskeletal modelling, data-model fusion and electromyography-informed modelling. *Interface Focus* **6**, 20150084 (2016).
14. Blemker, S. S., Asakawa, D. S., Gold, G. E. & Delp, S. L. Image-based musculoskeletal modeling: applications, advances, and future opportunities. *J. Magn. Reson. Imaging* **25**, 441–451 (2007).
15. Ma, Y., Xie, S. & Zhang, Y. A patient-specific EMG-driven neuromuscular model for the potential use of human-inspired gait rehabilitation robots. *Comput. Biol. Med.* **70**, 88–98 (2016).
16. Zhang, J., Zhong, Y. & Gu, C. Neural network modelling of soft tissue deformation for surgical simulation. *Artif. Intell Med.* **97**, 61–70 (2019).
17. Oliveri, H. et al. Planning acetabular fracture reduction using patient-specific multibody simulation of the hip. In *Proceedings Medical Imaging 2017: Image-Guided Procedures, Robotic Interventions, and Modeling*, vol. 10135, 697–702 (SPIE, 2017).
18. Dostal, W. F. & Andrews, J. G. A three-dimensional biomechanical model of hip musculature[J]. *J. Biomech.* **14**, 803–812 (1981).
19. Dostal, W. F. The prediction of coordinates of bony landmark and hip muscle attachment points. PhD Thesis. The University of Iowa (1979).
20. Jensen, R. H. & Davy, D. T. An investigation of muscle lines of action about the hip: a centroid line approach vs the straight line approach. *J. Biomech.* **8**, 103–110 (1975).
21. Campbell, J. Q. & Petrella, A. J. Automated finite element modeling of the lumbar spine: using a statistical shape model to generate a virtual population of models. *J Biomech.* **49**, 2593–2599 (2016).
22. Perez M. A. et al. Validation of bone remodelling models applied to different bone types using Mimics. PhD Thesis. University of Zaragoza, 2007.
23. Liu, Y. et al. Pelvic fracture segmentation using a multi-scale distance-weighted neural network. In: Medical Image Computing and Computer-Assisted Intervention – MICCAI 2023 Lecture Notes in Computer Science (Springer, 2023).
24. Wu, W., Han, Z., Hu, K. & Chen, C. Three-dimensional reconstructions in the spine and surgical-practice simulation on digital images: a step by step approach by using Mimics-Geomagic-3D Printing Methods. *Asian J. Surg.* **46**, 569–570 (2023).
25. Yibulayimu, S. et al. Pelvic fracture reduction planning based on morphable models and structural constraints. *International Conference on Medical Image Computing and Computer-Assisted Intervention*, 322–332 (Springer Nature, Cham, Switzerland, 2023).
26. Liu, J. et al. Sagittal support rather than medial cortical support matters in geriatric intertrochanteric fracture: a finite element analysis study. *Heliyon* **10**, e28606 (2024).
27. Shi, C. et al. Fast and precise collision detection for detailed and complex physiological structures. *Comput. Methods Programs Biomed.* **240**, 107707 (2023).
28. Clark, K. et al. The Cancer Imaging Archive (TCIA): maintaining and operating a public information repository. *J. Digit. Imaging* **ume 26**, 1045–1057 (2013). Decemberpp.
29. Han, R. et al. Atlas-based automatic planning and 3D-2D fluoroscopic guidance in pelvic trauma surgery. *Phys. Med. Biol.* **64**, 105025 (2019).
30. Audenaert, E. A. et al. Cascaded statistical shape model based segmentation of the full lower limb in CT. *Comput. Methods Biomech. Biomed. Eng.* **22**, 644–657 (2019).
31. Kim, K. & Lee, S. Vertebrae localization in CT using both local and global symmetry features. *Comput. Med. Imaging Graphics* **58**, 45–55 (2017).
32. Abdi, H. & Williams, L. J. Principal component analysis. *Wiley Interdiscip. Rev. Comput. Stat.* **2**, 433–459 (2010).

33. Albrecht, T., Lüthi, M., Gerig, T. & Vetter, T. Posterior shape models. *Med. Image Anal.* **17**, 959–973 (2013).
34. Brand, R. A. A model of lower extremity muscular anatomy. *J. Biomech. Eng.* **104**, 304 (1982).
35. Gluek, C., Zdero, R. & Quenneville, C. E. Evaluating the mechanical response of novel synthetic femurs for representing osteoporotic bone. *J Biomech* **111**, 110018 (2020).
36. Besl, P. J. & McKay, N. D. A method for registration of 3-D shapes. *IEEE Transact. Pattern Anal. Mach. Intell.* **14**, 239–256 (1992).
37. Buschbaum, J. et al. Computer-assisted fracture reduction: a new approach for repositioning femoral fractures and planning reduction paths. *Int. J. Comput. Assisted Radiol. Surg.* **10**, 149–159 (2015).
38. Ye, R. et al. A simple and novel hybrid robotic system for robot-assisted femur fracture reduction. *Adv. Robot.* **26**, 83–104 (2012).
39. Joung, S. et al. Hazard analysis of fracture-reduction robot and its application to safety design of fracture-reduction assisting robotic system. In *International Conference on Robotics and Automation*. 1554–1561 (IEEE, 2010).
40. Millard, M., Uchida, T., Seth, A. & Delp, S. L. Flexing computational muscle: modeling and simulation of musculotendon dynamics. *J. Biomech. Eng.* **135**, 021005 (2013).
41. Delp, S. L. et al. OpenSim: open-source software to create and analyze dynamic simulations of movement. *IEEE Trans. Biomed. Eng.* **54**, 1940–1950 (2007).
42. Liu, J et al. Enhancing preoperative planning for pelvic fracture reduction: rapid and precise patient-specific musculoskeletal modeling for improved safety and efficacy, mendeley data, V1 https://doi.org/10.17632/6m97r8p44s.1 (2025).
43. Thelen, D. G., Anderson, F. C. & Delp, S. L. Generating dynamic simulations of movement using computed muscle control. *J. Biomech.* **36**, 321–328 (2003).
44. Bresnahan, L., Fessler, R. G. & Natarajan, R. N. Evaluation of change in muscle activity as a result of posterior lumbar spine surgery using a dynamic modeling system. *Spine* **35**, E761–E767 (2010).
45. OpenSim. Scaling: How Scaling Works. OpenSim Documentation. Retrieved 2025/07/16 from https://opensim.org/documentation/
46. Ahmed, K. et al. Current status of robotic assisted pelvic surgery and future developments. *Int. J. Surg.* **7**, 431–440 (2009).
47. Fernandez, J. W. et al. Anatomically based geometric modelling of the musculo-skeletal system and other organs. *Biomech. Modelin Mechanobiol.* **2**, 139–155 (2004).
48. Kulis, B. Metric learning: a survey. *Foundations and Trends in Machine Learning* **5**, 287–364 (2013).
49. Jamwal, P. K., Hussain, S. & Ghayesh, M. H. Intrinsically compliant parallel robot for fractured femur reduction: Mechanism optimization and control. *Robot. Autonomous Syst.* **141**, 103787 (2021).
50. Joung, S. et al. A robot assisted hip fracture reduction with a navigation system. *Med. Image Comput. Comput. Assist. Interv.* **11**, 501–508 (2008).
51. Abedinnasab, M. H. et al. The wide-open three-legged parallel robot for long-bone fracture reduction. *J. Mech. Robot.* **9**, 015001 (2017).
52. Seth, A., Hicks, J. L. et al. OpenSim: simulating musculoskeletal dynamics and neuromuscular control to study human and animal movement. *PLoS Comput. Biol.* **14**, e1006223 (2018).
53. Seth, A., Sherman, M., Reinbolt, J. A. & Delp, S. L. OpenSim: a musculoskeletal modeling and simulation framework for in silico investigations and exchange. *Procedia IUTAM* **2**, 212–232 (2011).

Acknowledgements
We gratefully acknowledge the financial support provided by the National Key Research and Development Project (2024YFB4709903), the National Natural Science Foundation of China (NSFC52027806, 52435005), Beijing Scholar Training Program 2021, HuBei Province Key R&D Program (2023BCB152, 2024BCA004), Beijing Jishuitan Research Funding (ZR-202504) the Interdiciplinary Research Program of HUST 2024JCYJ010, 2024JCYJ043, 2025JCYJ062.

Author contributions
Jixuan Liu: Writing – review & editing, Writing – original draft, Methodology, Formal analysis, Data curation, Conceptualization. Yufeng Ge: Methodology, Conceptualization, Clinical data acquisition. Sutuke Yibulayimu: Software. Yanzhen Liu: Clinical data acquisition. Yuanwei Zheng: Illustration. Xinbao Wu*: Funding acquisition. Yu Wang*: Supervision.

Competing interests
The authors declare no competing interests.

Additional information
Supplementary information The online version contains supplementary material available at https://doi.org/10.1038/s43856-025-01238-2.

Correspondence and requests for materials should be addressed to Xinbao Wu or Yu Wang.

Peer review information *Communications Medicine* thanks Anna Ghidotti, Maxence Lavaill, Simone Borrelli and the other, anonymous, reviewer(s) for their contribution to the peer review of this work. A peer review file is available.